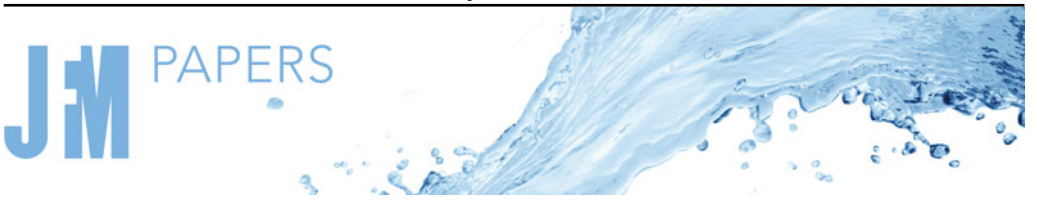
J. Fluid Mech. (2025), *vol.* 1008, A28, doi:10.1017/jfm.2025.136



Reflection of multiple incident shock waves and shock interaction train

Zhu-Di Li[1] **and Chen-Yuan Bai**[1]

[1]Ministry of Education Key Laboratory of Fluid Mechanics, Beihang University, Beijing 100191, PR China

Corresponding author: Chen-Yuan Bai, baicy@buaa.edu.cn

(Received 3 September 2024; revised 6 January 2025; accepted 26 January 2025)

The reflection of multiple incident shock waves that converge to a single point on the reflecting surface is studied in this paper. The number of the incident shocks, denoted K, is arbitrary. The interaction between the reflected shock of one incident shock and the other incident shocks may produce various possible configurations, such as type-I, type-II and type-IV shock interferences. The number of possible reflection configurations is shown to be an exponential function of $(K-1)$ with base 2. The possibility of pre-, middle- and post-Mach reflections, which means Mach reflection occurs for the first, middle and last incident shock, is revealed through numerical simulation for $K=3$. For the particular case where the incident shocks are produced by equal variation of wedge surface deflection, the conventional von Neumann condition and detachment condition for the kth incident shock to have Mach reflection are derived. It is shown that the von Neumann condition for regular reflection is lowered and the detachment condition for Mach reflection is elevated as k increases. The shock reflection patterns for $K=1, 2, \ldots, 10$ are obtained by numerical simulations. We observe a shock interaction train structure, where we have pre-Mach reflection followed by $(K-1)$ type-I or type-II shock interferences. We also observe that the Mach stem height decreases with K well above the von Neumann condition and becomes non-monotonic near the von Neumann condition.

Key words: high-speed flow, shock waves, supersonic flow

1. Introduction

Shock reflection is a typical phenomenon in supersonic flow and has been well studied for single incident shock reflection before (Ben-Dor 2007). When supersonic flow with an inflow Mach number $M_0 > 1$ encounters a wedge with the lower wedge surface turning at an angle θ_w, an incident shock wave is produced, which will reflect over the reflecting surface. Both regular reflection (RR) and Mach reflection (MR) are possible, depending on M_0 and θ_w. For RR, the incident shock wave only produces a reflected shock wave.

© The Author(s), 2025. Published by Cambridge University Press.

https://doi.org/10.1017/jfm.2025.136 Published online by Cambridge University Press

For MR, first observed by Mach (1878), the reflection of the incident shock wave produces a reflected shock wave and a strong shock wave named the Mach stem. A triple point connects these three shock waves and issues a slipline. The three shock waves and the slipline separate the flow structure into four regions, the solutions of which in the vicinity of the triple point can be solved by the three-shock theory of von Neumann (1943, 1945). In the M_0–θ_w plane, there are two transition curves: the von Neumann condition, below which only RR is possible, and the detachment condition, above which only MR is possible. The region between these two curves is called the double solution domain, where both reflections are possible (Hornung, Oertel & Sandeman 1979; Chpoun *et al.* 1995; Vuillon, Zeitoun & Ben-Dor 1995; Ivanov *et al.* 2001; Ben-Dor *et al.* 2002).

When the number of incident shocks exceeds one, the problem becomes far more complex. For the special case of reflection with two incident shock waves, the following phenomena have been observed by recent studies (Guan, Bai & Wu 2018, Guan, Bai & Wu 2020, Guan *et al.* 2020):

(*a*) both pre-Mach reflection (the first incident shock wave has Mach reflection) and post-Mach reflection (the second incident shock wave has Mach reflection) can be produced;
(*b*) for pre-Mach reflection, the second incident shock wave elevates the Mach stem and may induce inverse Mach reflection below the von Neumann condition. Additionally, the reflected shock of the first incident shock may interact with the second incident shock, producing either type-I or type-II shock interference, resulting in four possible reflection configurations;
(*c*) for post-Mach reflection, the first incident shock wave intersects the Mach stem to produce a type-IV shock interference, which produces a jet penetrating into the flow duct below the slipline.

For the extreme case with an infinite number of incident weak shock waves, isentropic compression waves can be used to approximate these shock waves. The reflection of a centred compression wave can be considered as a limiting case of reflection of multiple incident shocks that converge at the same point on the reflection surface. According to the study on this problem (Bai 2024), the double solution domain, with both regular and Mach reflections, of centred compression wave reflection is enlarged compared with single shock reflection. In this case, no clear triple point structure exists, instead, the reflected shock and Mach stem form a smooth curved shock wave.

The study of these two extreme cases (one with two incident shocks and the other with an infinite number of weak incident shocks) demonstrates that increasing the number of incident shocks not only alters the transition conditions but also changes the Mach reflection configuration.

Inlet compression with a single shock reflection suffers from total pressure loss due to the strong shock wave. Isentropic compression has been used in the design of the Busemann inlet (Busemann 1942); however, the full Busemann intake has a very long axial length, which causes heavy viscous losses due to the long boundary layer (Ogawa *et al.* 2015). It may be advantageous to consider the intermediate case of using compression by multiple shock waves. Before exploring whether such a design can avoid total pressure loss, it is necessary to study the fundamental question of shock reflection with multiple incident shock waves. In this study, we consider multiple incident shock reflection with a finite number K of incident shocks. Figure 1 is a schematic display of shock reflection with multiple incident shocks compared with a single incident shock. In figure 1(*b*), the turning

https://doi.org/10.1017/jfm.2025.136 Published online by Cambridge University Press

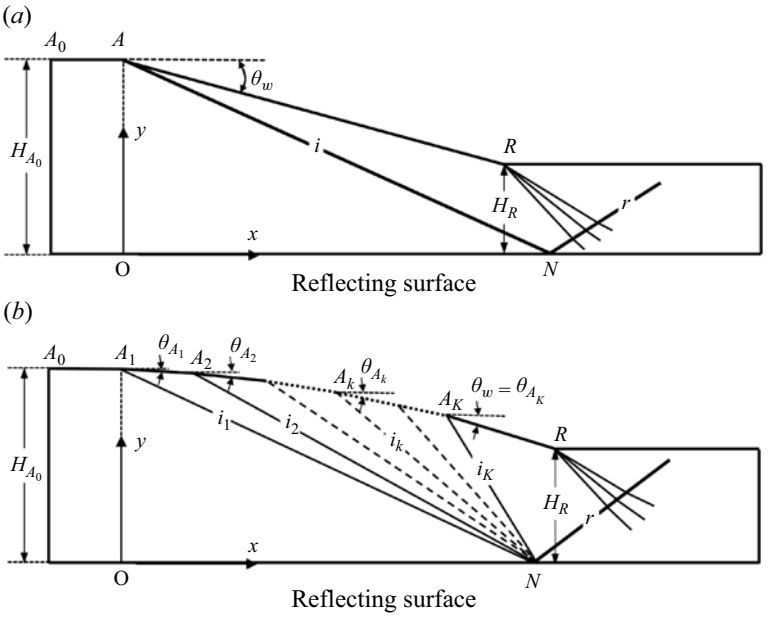


Figure 1. Reflection configuration (only regular reflection is shown in this figure): (*a*) single shock reflection; (*b*) multiple shock reflection.

points are labelled as $A_1, A_2, \ldots, A_K$ and the angle between each wedge lower surface and the horizontal line is labelled as $\theta_{A_1}, \theta_{A_2}, \ldots, \theta_{A_K}$ (wedge deflection angle) and the total wedge deflection angle is labelled as $\theta_w (= \theta_{A_K})$. For the multiple incident shock case, a series of incident shocks, labelled $i_1, i_2, \ldots, i_K$ in figure 1(*b*), with each produced by a local turning of the lower wedge surface, reflect over the reflecting surface. If these incident shocks reflect over the reflecting surface at different points, then each reflection may be considered independently. In this paper, we only consider the case where all the incident shocks reflect at the same point (denoted N in figure 1*b*). This study bridges the previous studies for two extreme cases: $K \leqslant 2$ and $K \to \infty$. In § 2, we consider the general case where each incident shock has arbitrary strength and estimate the number of possible reflection configurations by counting the possible number of local reflection types at each interaction point. Following the study by Guan *et al.* (2020) for two incident shocks, type-IV shock interference is one possible local structure when a Mach stem of an incident shock interacts with the upstream incident shocks. Accounting for this possibility, we estimate all reflection configurations in § 2.1. We will also use the case $K = 3$ to show that, apart from pre-Mach reflection and post-Mach reflection, middle-Mach reflection is also possible in § 2.2. This numerical result indicates a similarity between two different ways of describing the local reflection configuration: type-IV shock interference and type-II shock interference. This similarity analysis will allow us to estimate the number of possible reflection configurations differently in § 2.3.

In § 3, we consider the specific case where the incident shocks are produced by equal variation of (a series of) wedge surface deflection angles. We will derive the conventional von Neumann condition and the detachment condition for each incident shock. The results will be compared with the single incident shock case and the centred compression wave case. Additionally, we provide the numerical results for $K = 1$ to $K = 10$ to observe how the reflection configuration depend on K.

https://doi.org/10.1017/jfm.2025.136 Published online by Cambridge University Press

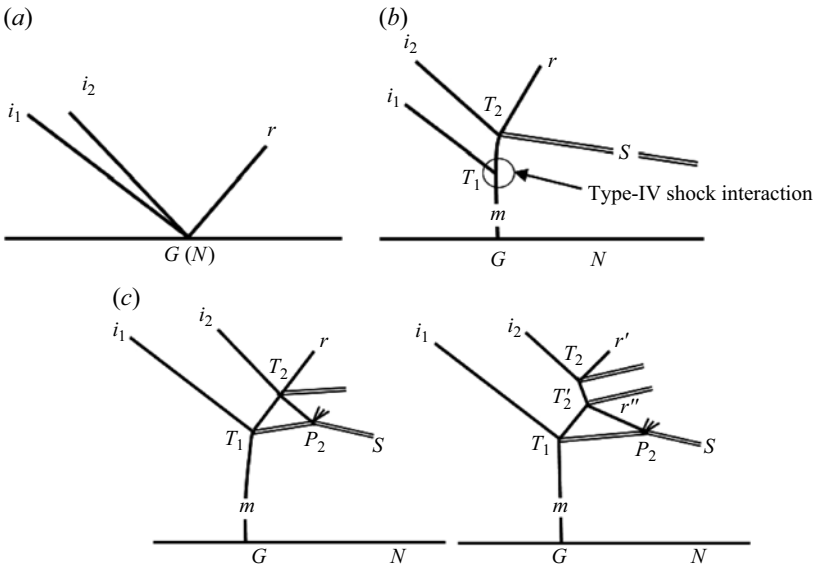


Figure 2. Reflection configurations for two incident shocks: (*a*) regular reflection; (*b*) post-Mach reflection; (*c*) pre-Mach reflection with type-I or type-II shock interferences.

In § 4, the concluding remarks are provided.

2. Possibilities of shock reflection configuration with multiple incident shocks

2.1. *An intuitive estimation of the number of possible reflection configurations*

The number of possible reflection configurations can be estimated based on observations from shock reflection with two incident shock waves. According to previous studies (Guan *et al.* 2018, 2020; Guan *et al.* 2020), apart from regular reflection, either the first incident shock or the second incident shock may have Mach reflection. Figure 2 displays all the possibilities. For pre-Mach reflection, as illustrated in figure 2(*c*), the reflected shock of the first incident shock may interact with the second incident shock to generate either type-I or type-II shock interference (Guan *et al.* 2020). For post-Mach reflection, as illustrated in figure 2(*b*), the first incident shock interacts with the Mach stem of the second incident shock to generate type-IV shock interference. According to Guan *et al.* (2020), pre-Mach reflection, in which the first incident shock wave has Mach reflection, occurs when the first incident shock is much stronger than the second one, and post-Mach reflection, in which the downstream incident shock wave has Mach reflection, occurs when the second incident shock is relatively stronger. It is difficult to provide transition conditions to produce these two types of reflection, since inverse Mach reflection may occur.

Thus, even for the reflection with only two incident shock waves, we may have four possibilities:

(1) regular reflection, as shown in figure 2(*a*);
(2) pre-Mach reflection with type-I shock interference and pre-Mach reflection with type-II shock interference (figure 2*c*);
(3) post-Mach reflection with type-IV shock interference (figure 2*b*).

Now, we consider the reflection with three incident shock waves. Inspired by observations from two incident shock waves, the following configurations are possible:

https://doi.org/10.1017/jfm.2025.136 Published online by Cambridge University Press

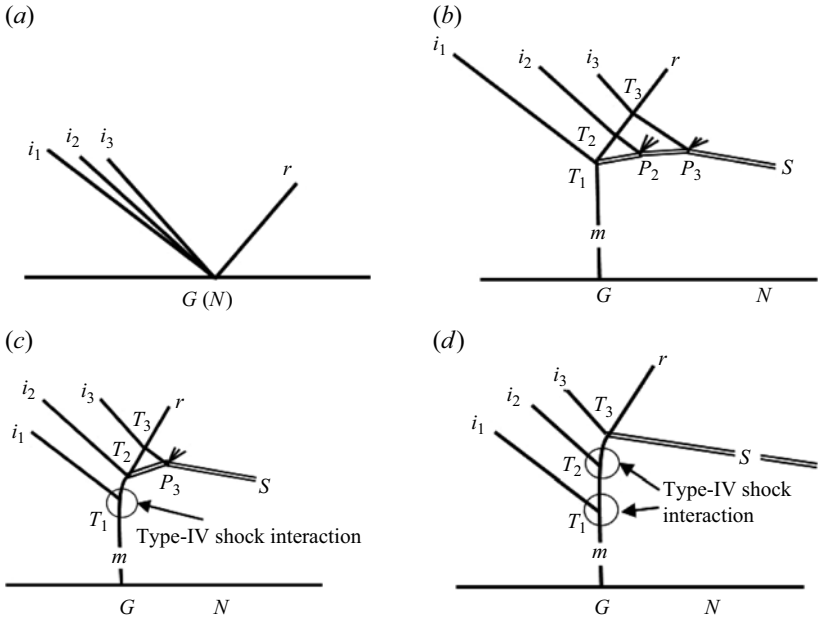


Figure 3. Reflection configurations: (*a*) regular reflection; (*b*) pre-Mach reflection; (*c*) middle-Mach reflection; (*d*) post-Mach reflection.

(1) regular reflection (figure 3*a*);
(2) first incident shock Mach reflection or pre-Mach reflection (figure 3*b*), with type-I or type-II shock interferences at both interaction points T_2 and T_3, i.e. there are four possibilities for this case;
(3) second incident shock Mach reflection or middle-Mach reflection (figure 3*c*), with type-I or type-II shock interference at interaction point T_3, and with type-IV shock interference at interaction point T_1, i.e. there are two possibilities for this case;
(4) third incident shock Mach reflection or post-Mach reflection (figure 3*d*), with type-IV shock interferences at interaction points T_1 and T_2, i.e. there is one possibility for this case.

Thus, there are eight possible reflection configurations for three incident shock waves. Now consider K incident shock waves. We possibly have:

(1) one regular reflection;
(2) first incident shock Mach reflection or pre-Mach reflection, with 2^{K-1} type-I or type-II shock interferences at interaction points T_2, T_3,. . .,T_K;
(3) second incident shock Mach reflection, with 2^{K-2} type-I or type-II shock interferences at interaction points T_3,T_4,. . .,T_K, and with type-IV shock interference at interaction point T_1, i.e. in total, there are 2^{K-2} possibilities in this case;
(4) third incident shock Mach reflection, with 2^{K-3} type-I or type-II shock interferences at interaction points T_4,T_5,. . .,T_K, and with type-IV shock interferences at interaction points T_1 and T_2, i.e. in total, there are 2^{K-3} possibilities in this case;
(5) kth incident shock Mach reflection, with 2^{K-k} type-I or type-II shock interferences at interaction points T_{k+1},T_{k+2},. . .,T_K, and with type-IV shock interferences at interaction points T_1,T_2,. . .,T_{k-1}, i.e. in total, there are 2^{K-k} possibilities in this case.

https://doi.org/10.1017/jfm.2025.136 Published online by Cambridge University Press

Case	θ_{A_1} (deg)	θ_{A_2} (deg)	θ_{A_3} (deg)
1	10	20	30
2	5	25	30
3	5	10	30

Table 1. Three cases for numerical simulations, with $M_0 = 4$, $\theta_w = 30°$, $g = 0.4$.

Mesh	Grid points	H_{T_1}
A	800×200	0.1468
B	1200×300	0.1414
C	1600×400	0.1415

Table 2. Mach stem height for different meshes.

(6) Kth incident shock Mach reflection or post-Mach reflection, with type-IV shock interferences at interaction points T_1,T_2,. . .,T_{K-1}, i.e. in total, there is one possibility in this case.

Now, we can evaluate the total number (denoted N_p) of possibilities by summing up the numbers of possibilities for $k = 1, 2, \ldots, K$, i.e.

$$N_p = 1 + \sum_{k=1}^{K} 2^{K-k} = 1 + 2^K \sum_{k=1}^{K} \frac{1}{2^k}. \tag{2.1}$$

Inserting the obvious expression

$$\sum_{k=1}^{K} \frac{1}{2^k} = 1 - \left(\frac{1}{2}\right)^K \tag{2.2}$$

into (2.1) gives

$$N_p = 2^K. \tag{2.3}$$

This shows an exponential increase of N_p when K increases.

2.2. *Numerical results for $K = 3$*

Now, we display numerical results for multiple incident shock reflections with $K = 3$. The purpose of the simulation is to show that we can produce pre-Mach reflection, middle-Mach reflection and post-Mach reflection, depending on the strengths of the three incident shock waves or the wedge deflection angles θ_{A_1}, θ_{A_2} and θ_{A_3}. The paramaters $M_0 = 4$, $\theta_w = 30°$ and $g = 0.4$ (the relative wedge trailing edge height, defined by $g = H_R/H_{A_0}$) are shown in table 1. This condition frequently appears in papers related to single shock wave reflection and centred compression wave reflection.

Numerical simulations are carried out for the compressible Euler equations in gas dynamics, using a second-order Roe scheme on a structure grid, in a similar way as by Bai (2024). To ensure the accuracy of numerical results, we perform a grid convergence study using three different grids of increasing density for $M_0 = 4$, $\theta_w = 30°$, $g = 0.4$ and $K = 3$. Mesh A has 800 × 200 grid points, Mesh B has 1200 × 300 grid points and Mesh

https://doi.org/10.1017/jfm.2025.136 Published online by Cambridge University Press

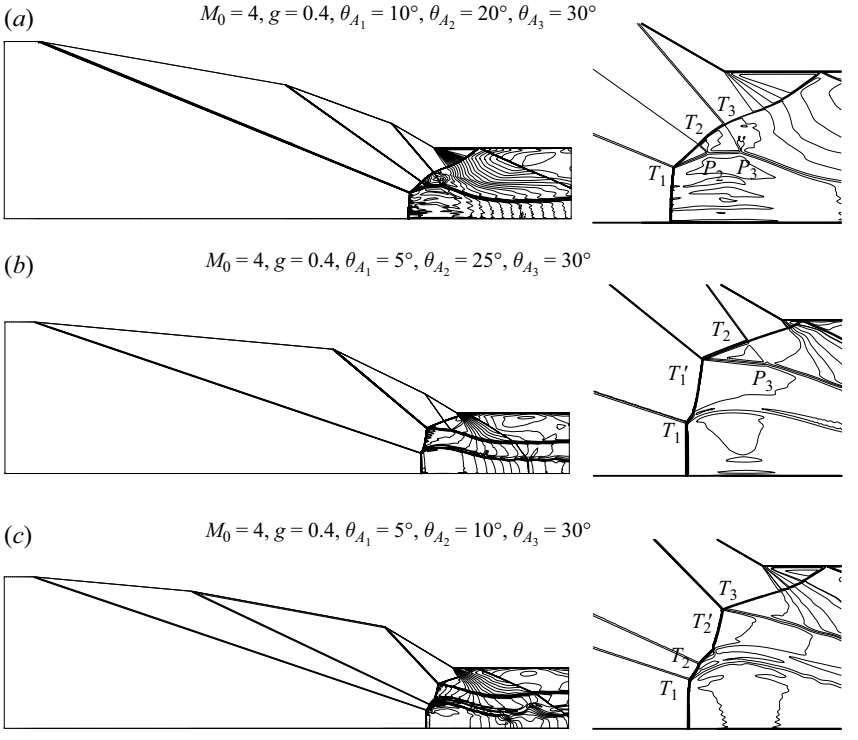


Figure 4. Mach contourlines for $M_0 = 4$ and $\theta_w = 30°$: (*a*) Case 1; (*b*) Case 2; (*c*) Case 3.

C has 1600 × 400 grid points. Table 2 shows the influence of grid density on the distance from T_1 as shown in figure 3 to the reflecting surface (denoted as H_{T_1}). It can be seen that H_{T_1} for Mesh B and Mesh C are very close, so we will use a mesh as dense as Mesh B in the following computations.

Case 1 has a large variation of wedge surface deflection angle θ_{A_1}. Case 2 has a small variation of wedge surface deflection angle θ_{A_1}, but a large variation of wedge surface deflection angle $(\theta_{A_2} - \theta_{A_1})$. Case 3 has a small variation of wedge surface deflection angles θ_{A_1} and $(\theta_{A_2} - \theta_{A_1})$, but a large variation of wedge surface deflection angle $(\theta_{A_3} - \theta_{A_2})$. A large variation of wedge surface deflection angle is supposed to induce Mach reflection easier.

The Mach contour lines from the numerical simulations and the enlarged views are all displayed in figure 4. We observe pre-Mach reflection for Case 1, middle-Mach reflection for Case 2 and post-Mach reflection for Case 3.

As seen from the numerical result shown in figure 4(*a*), Case 1 produces a pre-Mach reflection, even though the first incident shock has a wedge deflection angle θ_{A_1} below the conventional von Neumann condition. Figure 4(*a*) also shows an enlarged view around triple point T_1, where the first incident shock has an inverse Mach reflection, meaning the Mach stem is convex towards the upstream direction. The inverted shock only occurs when the flow condition is in the domain below the conventional von Neumann condition (Hekiri & Emanuel 2015). This inverse Mach reflection has also been observed in the case of two incident shock waves and is explained using the blunt-body analogy (Guan *et al.* 2018). The blunt-body analogy comes from the observation of Roye, Henderson & Menikoff (1998), who provided a configuration (see their figure 6*b*) where an additional blunt body is placed along the reflecting surface and an inverted Mach reflection ahead of this blunt body is observed. The slipline deflects towards the upward direction. The second

https://doi.org/10.1017/jfm.2025.136 Published online by Cambridge University Press

incident shock interacts with the reflected shock from triple point T_1 to produce a type-I shock interference at interaction point T_2. Guan *et al.* (2018) showed that type-II shock interference may exist in the case of two incident shock waves. One reflected shock from T_2 reflects again over the slipline at point P_2, to produce an expansion fan and drive the slipline to change direction, for the reason of pressure balance as discussed by Guan *et al.* (2018) for two incident shock waves. Another reflected shock from point T_2 interacts with the third incident shock at point T_3 to produce another type-I shock interference, and one reflected shock from T_3 further reflects over the slipline at point P_3 to produce another expansion fan and change the slope of the slipline in a similar way as at point P_2. The slipline is driven towards the downward direction, so that a convergent-divergent quasi-one-dimensional flow duct can be sustained.

As seen from the numerical result shown in figure 4(*b*), Case 2 produces a middle-Mach reflection, which means that the second incident shock generates a Mach reflection. Figure 4(*b*) also offers an enlarged view around the interaction points. The second incident shock has a Mach reflection, and the slipline from triple point T_2 is deflected downwards. In addition, since the incoming flow for the second incident shock is not horizontal, it is difficult to estimate whether it is a reverse Mach reflection from figure 4(*b*). The first incident shock interacts with the Mach stem from triple point T_2 to produce a type-IV shock interference at interaction point T_1. The type-IV shock interference consists of two triple points (T_1 and $T_1^{'}$) and a jet zone (surrounded by the sliplines from the triple points T_1 and $T_1^{'}$), which has also been observed in the case of two incident shock waves (Guan *et al.* 2020). As for the third incident shock, it interacts with the reflected shock from triple point T_2 to produce a type-I shock interference at interaction point T_3.

As seen from the numerical result shown in figure 4(*c*), Case 3 produces a post-Mach reflection. The flow structure in this case differs from that in Cases 1 and 2, and is magnified in figure 4(*c*) around the interaction points. The third incident shock has a Mach reflection, and the slipline from triple point T_3 is deflected downwards. It is difficult to estimate whether it is a reverse Mach reflection from figure 4(*c*) as in Case 2. The second incident shock interacts with the Mach stem from triple point T_3 to produce a type-IV shock interference at interaction point T_2, which consists of two triple points (T_2 and $T_2^{'}$) and a jet zone (surrounded by the sliplines from triple points T_2 and $T_2^{'}$).

2.3. *Similarity of apparent different reflection configurations and equivalent number of possible configurations*

In § 2.1, for the shock reflection problem with K incident shock waves, we have assumed that if the kth incident shock has Mach reflection, then there are 2^{K-k} type-I or type-II shock interferences at interaction points T_{k+1},T_{k+2},. . .,T_K, and type-IV shock interferences at interaction points T_1,T_2,. . .,T_{k-1}.

There are 2^{K-k} possibilities for each k, resulting in $N_p = 2^K$ possibilities in total. For the special case of $K = 3$ as considered in § 2.2, $N_p = 8$.

However, as seen from figure 4(*b*) or figure 4(*c*), there are two equivalent ways to count the number of configurations. We only consider Case 2 (figure 4*b*) to illustrate this equivalence.

The original way, as discussed in § 2.1, considers the second incident shock generating a Mach reflection (middle-Mach reflection) and the first incident shock interacting with the Mach stem of the middle-Mach reflection, thereby generating a type-IV shock interference.

The equivalent way is to regard the first incident shock as generating a Mach reflection (pre-Mach reflection) and the second incident shock interacting with the reflected shock

https://doi.org/10.1017/jfm.2025.136 Published online by Cambridge University Press

K	N_p	M_p
1	2	2
2	4	3
3	8	5
5	32	17
10	1024	513
20	1 048 576	524 289

Table 3. Dependence of N_p and M_p on K.

of the pre-Mach reflection, so as to generate a type-II shock interference. The same is true for Case 3 as shown in figure 4(*c*) and for more general situations.

Now, we use the equivalent way to recount the number of possibilities of shock reflection. We have:

(1) one regular reflection, as before;
(2) first incident shock Mach reflection or pre-Mach reflection, with 2^{K-1} type-I or type-II shock interferences at interaction points $T_2,T_3,\ldots,T_K$. This can be viewed as a pre-Mach reflection followed by a series type-I or type-II shock interferences;
(3) second incident shock Mach reflection, with 2^{K-2} type-I or type-II shock interferences at interaction points $T_3,T_4,\ldots,T_K$, and with a pre-Mach reflection at T_1 and a type-II (previously regarded as type-IV interference at T_1 and a Mach reflection at T_2) shock interference at T_2. In summary, this reflection can be viewed as a pre-Mach reflection, followed by a type-II shock interference and then by $(K-2)$ type-I or type-II shock interferences;
(4) third incident shock Mach reflection, for similar reasons as above, can be viewed as a pre-Mach reflection, followed by two type-II shock interferences and then by $(K-3)$ type-I or type-II shock interferences.
(5) kth incident shock Mach reflection, for similar reasons as above, can be viewed as a pre-Mach reflection, followed by $(k-1)$ type-II shock interferences and then by $(K-k)$ type-I or type-II shock interferences;
(6) Kth incident shock Mach reflection, this can be seen as a pre-Mach reflection followed by $(K-1)$ type-II interference structures.

It is obvious that the possibilities for the second to Kth incident shock Mach reflections are all covered by the first incident shock Mach reflection, so the total number, denoted as M_p, of possibilities is simply given as

$$M_p = 1 + 2^{K-1}. \tag{2.4}$$

Table 3 provides a comparison between the number of reflection types given by (2.3) and by (2.4). It is seen that the equivalent number is highly reduced compared with the original estimation for very large K. Since $\frac{1+2^{K-1}}{2^K} \approx \frac{1}{2}$ when K is large enough, the number M_p is approximately half of N_p.

3. Multiple shock reflection for equal variation of a series of wedge surface deflection

3.1. *Geometric conditions for equal variation of deflection angle problem*

Consider K incident shock waves, labelled as i_k with $k = 1, 2, \ldots K$, produced by an equal variation of deflection angle $\Delta\theta_w = \theta_w/K$, at turning points A_k with $k = 1, 2, \ldots, K$.

https://doi.org/10.1017/jfm.2025.136 Published online by Cambridge University Press

First, we will consider the shock properties for each incident shock.

The shock angle β_{A_k} for shock i_k satisfies the shock relation (for weak solution)

$$\tan \Delta\theta_w = f_\theta(M_{k-1}, \beta_{A_k}), \quad k = 1, 2, \ldots, K \tag{3.1}$$

and

$$f_\theta(M, \beta) = \frac{2\left(M^2 \sin^2\beta - 1\right)}{\left(M^2\left(\gamma + \cos 2\beta\right) + 2\right)\tan\beta}. \tag{3.2}$$

The Mach number M_k between shock i_k and shock i_{k+1} is given by the shock relation for Mach number

$$M_k = f_M(M_{k-1}, \beta_{A_k}), \quad k = 1, 2, \ldots, K, \tag{3.3}$$

where

$$f_M(M, \beta) = \sqrt{\frac{(\gamma - 1)M^2 + 2}{2\gamma M^2 \sin^2\beta - (\gamma - 1)} + \frac{2M^2\cos^2\beta}{(\gamma - 1)M^2 \sin^2\beta + 2}}. \tag{3.4}$$

The pressure between shock i_k and shock i_{k+1} is given by the shock relation for pressure

$$p_k = p_{k-1} f_p(M_{k-1}, \beta_{A_k}), \quad k = 1, 2, \ldots, K, \tag{3.5}$$

where

$$f_p(M, \beta) = 1 + \frac{2\gamma}{\gamma + 1}\left(M^2 \sin^2\beta - 1\right). \tag{3.6}$$

Now consider the coordinates of A_k.

In this paper, the incident shock waves are required to intersect at a common point $N(x_N, 0)$ on the reflecting surface, with x_N determined by

$$x_N = \frac{y_{A_1}}{\tan\beta_{A_1}} = \frac{H_{A_0}}{\tan\beta_{A_1}}. \tag{3.7}$$

Due to this constraint, the horizontal position x_{A_k} of A_k satisfies the following relations:

$$\begin{cases} x_{A_1} = 0, \\ x_{A_{k+1}} = x_N - \dfrac{y_{A_{k+1}}}{\tan\left(\beta_{A_{k+1}} + k\Delta\theta_w\right)}, \quad k = 1, 2, \ldots, K-1. \end{cases} \tag{3.8}$$

The vertical position y_{A_k} at each turning point satisfies the following obvious geometrical relations:

$$\begin{cases} y_{A_1} = H_{A_0}, \\ y_{A_k} - y_{A_{k+1}} = \left(x_{A_{k+1}} - x_{A_k}\right)\tan\left(k\Delta\theta_w\right), \quad k = 1, 2, \ldots, K-1. \end{cases} \tag{3.9}$$

When x_{A_k} and y_{A_k} are given or solved, then (3.8) and (3.9) can be used to give the relations

$$x_{A_{k+1}} = \frac{y_{A_k} + x_{A_k}\tan\left(k\Delta\theta_w\right) - x_N\tan\left(\beta_{A_{k+1}} + k\Delta\theta_w\right)}{\tan\left(k\Delta\theta_w\right) - \tan\left(\beta_{A_{k+1}} + k\Delta\theta_w\right)} \tag{3.10}$$

and

$$y_{A_{k+1}} = \left(x_N - x_{A_{k+1}}\right)\tan\left(\beta_{A_{k+1}} + k\Delta\theta_w\right) \tag{3.11}$$

for $x_{A_{k+1}}$ and $y_{A_{k+1}}$, respectively.

https://doi.org/10.1017/jfm.2025.136 Published online by Cambridge University Press

When $\Delta\theta_w \to 0$ and $K \to \infty$, all the incident shock waves will be compression Mach waves and we recover the situation considered by Bai (2024).

3.2. *Conventional detachment condition and von Neumann condition for the kth incident shock*

For reflection of a single shock wave, the transition between the regular reflection and the Mach reflection is determined by the conventional detachment condition and von Neumann condition. When $K \to \infty$, the problem reduces to the reflection of a centred compression wave. It has been shown that the double solution domain, which includes both regular and Mach reflections, is enlarged in the case of centred compression wave reflection compared with single incident shock reflection (Bai 2024). Now, we look at how the transition conditions depend on k for finite values of incident shock waves.

Given M_0 and the wedge deflection angles θ_{A_k} at the wedge turning points A_k, the Mach number M_k and pressure p_k in region (k) (downstream of the kth incident shock wave) are obtained by solving the shock relations (3.1)–(3.5), recursively up to k.

First, we consider the detachment condition.

For a given M_0, the detachment condition for the kth incident shock, denoted as $\theta_{A_k} = \theta_{A_k}^{(D)}(M_0)$, is here equal to the value of θ_{A_k} such that the flow deflection angle for the reflected shock of the kth incident shock reaches the detachment angle. If the first to kth incident shocks reflect as a whole to produce regular reflection, then the flow parameters in the region downstream of the reflected shock (with shock angle $\beta_{r,k}$), denoted as region (2), are given by the oblique shock wave relations with flow deflection angle θ_{A_k}

$$\begin{cases} \tan\theta_{A_k} = f_\theta(M_k, \beta_{r,k}) \\ M_{2,k} = f_M(M_k, \beta_{r,k}) \\ p_{2,k} = p_1 f_p(M_k, \beta_{r,k}) \end{cases}. \tag{3.12}$$

The detached angle of the kth incident shock is $\theta_{A_k} = \theta_{max}(M_k)$ with θ_{max} determined by

$$\tan\theta_{max} = f_\theta(M_k, \beta_{m,k}), \tag{3.13}$$

where $\beta_{m,k}$ is the shock angle of the reflected shock at the condition of detachment and satisfies

$$\sin^2\beta_{m,k} = \frac{1}{\gamma M_k^2}\left(\frac{\gamma+1}{4}M_k^2 - 1 + \sqrt{(1+\gamma)(1+\frac{\gamma-1}{2}M_k^2 + \frac{\gamma+1}{16}M_k^4)}\right). \tag{3.14}$$

Now, we consider the von Neumann condition.

The von Neumann condition is here defined as the condition for θ_{A_k}, denoted as $\theta_{A_k} = \theta_{A_k}^{(N)}(M_0)$, such that the pressure $p_{2,k}$ downstream of the reflected shock of the kth incident shock (determined by (3.12)) is equal to the pressure p_N downstream of a normal shock wave connecting to the incoming flow, i.e.

$$p_{2,k} = p_N = p_0 f_p(M_0, \frac{\pi}{2}), \tag{3.15}$$

where f_p is given by (3.6).

The transition criteria in the M_0–θ_{A_k} plane for the kth incident shock to have Mach reflection are displayed in figure 5.

The curves for $k = 1$ correspond to the conventional detachment condition (labelled as 1_{st}^D in figure 5) and the von Neumann condition (labelled as 1_{st}^N in figure 5) for the shock reflection of the first incident shock.

https://doi.org/10.1017/jfm.2025.136 Published online by Cambridge University Press

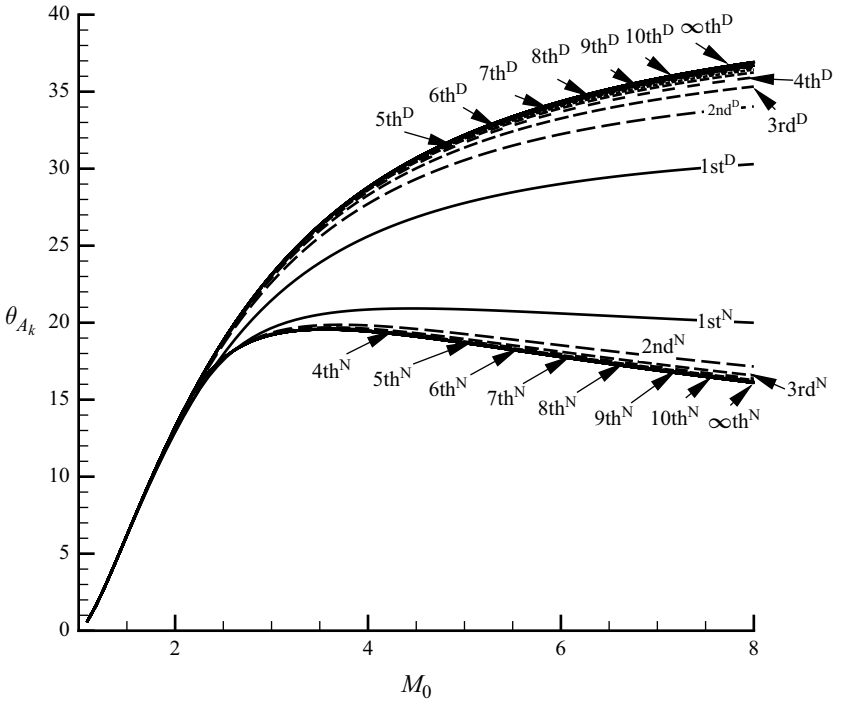


Figure 5. Transition criteria in the $M_0-\theta_{A_k}$ plane for the kth incident shock.

The curves for $k = 2$ correspond to the conventional detachment condition (labelled as 2^D_{nd} in figure 5) and the von Neumann condition (labelled as 2^N_{nd} in figure 5) for the shock reflection of the second incident shock, and the domain between the detachment condition and the von Neumann condition is larger than the domain for the first incident shock.

The curves for any k correspond to the conventional detachment condition (labelled as k^D_{th} in figure 5) and the von Neumann condition (labelled as k^N_{th} in figure 5) for the shock reflection of the kth incident shock, and the domain between the detachment condition and the von Neumann condition becomes larger with the increase of k.

The curves for $k \to \infty$ correspond to the conventional detachment condition (labelled as ∞^D_{th} in figure 5) and von Neumann condition (labelled as ∞^N_{th} in figure 5) for the reflection of a centred compression wave studied by Bai (2024).

From figure 5, as k increases, the changes in the von Neumann conditions and detachment conditions tend to slow down, because the intensity of the incident shock wave decreases significantly with the increase of k. When k reaches a certain level, the incident shock wave can even be regarded as a Mach wave. It is also shown that the von Neumann condition for regular reflection is lowered and the detachment condition for Mach reflection is elevated as k increases.

Note that figure 5 only provides the von Neumann condition and the detachment condition for the kth incident shock, and these conditions do not consider the effect of interferences by other incident shock waves.

For the same incoming Mach number, to achieve the same flow deflection angle, multiple shock wave compression with a larger k results in a larger pressure jump and a smaller Mach number decrease, meaning that increasing k and decreasing flow deflection angle achieve the same effect on pressure jump and Mach number decrease. As a result, the transition curves for reflection with a larger k could be seen as a shift to the left and

https://doi.org/10.1017/jfm.2025.136 Published online by Cambridge University Press

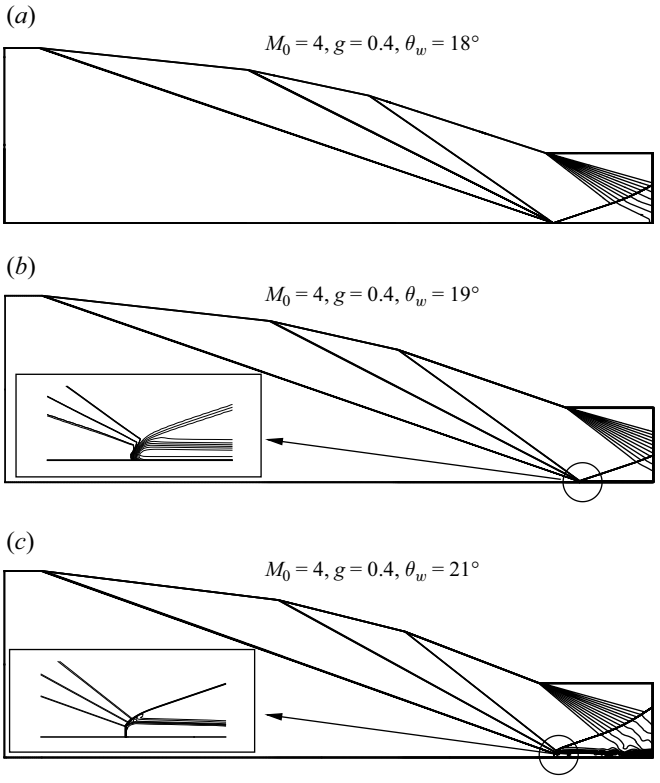


Figure 6. Mach contours with three incident shock waves for $M_0 = 4$: (*a*) $\theta_w = 18°$; (*b*) $\theta_w = 19°$; (*c*) $\theta_w = 21°$.

compression of the transition curves for reflection with a smaller k, and thus enlarging the double solution domain at the same abscissa.

In § 2, we have considered numerical results for multiple incident shock reflections for $M_0 = 4$, $g = 0.4$ and $K = 3$. Here, we still consider these parameters but with equal variation of deflection angle to check the critical conditions shown in figure 5.

First, consider the von Neumann condition. According to figure 5, the von Neumann conditions are $\theta_{A_1}^{(N)} = 20.85°$ for the first incident shock, $\theta_{A_2}^{(N)} = 19.82°$ for the second incident shock and $\theta_{A_3}^{(N)} = 19.61°$ for the third incident shock.

Figure 6(*a*) displays the numerical results for $\theta_{A_1} = 6°$, $\theta_{A_2} = 12°$ and $\theta_{A_3} = 18°$, which are all below the von Neumann conditions for the corresponding incident shocks. As shown in figure 6(*a*), we only observe regular reflection, as suggested by the transition conditions.

Figure 6(*b*) displays the numerical results for $\theta_{A_1} = 6.33°$, $\theta_{A_2} = 12.66°$ and $\theta_{A_3} = 19°$, which are also below the von Neumann conditions for the corresponding incident shocks. However, as shown in figure 6(*b*), the first incident shock produces a Mach reflection even though the wedge deflection angle $\theta_{A_1} = 6.33°$ for the first incident shock is well below the von Neumann condition $\theta_{A_1}^{(N)} = 20.85°$. The reason for the advance of transition from regular to Mach reflection is the same as discussed in § 2.2: the blunt-body effect of the downstream incident shock triggers this Mach reflection.

Figure 6(*c*) displays the numerical results for $\theta_{A_1} = 7°$, $\theta_{A_2} = 14°$ and $\theta_{A_3} = 21°$. The wedge deflection angles for the first and second incident shocks are both below the von Neumann conditions, but the wedge deflection angle for the third incident shock is above

https://doi.org/10.1017/jfm.2025.136 Published online by Cambridge University Press

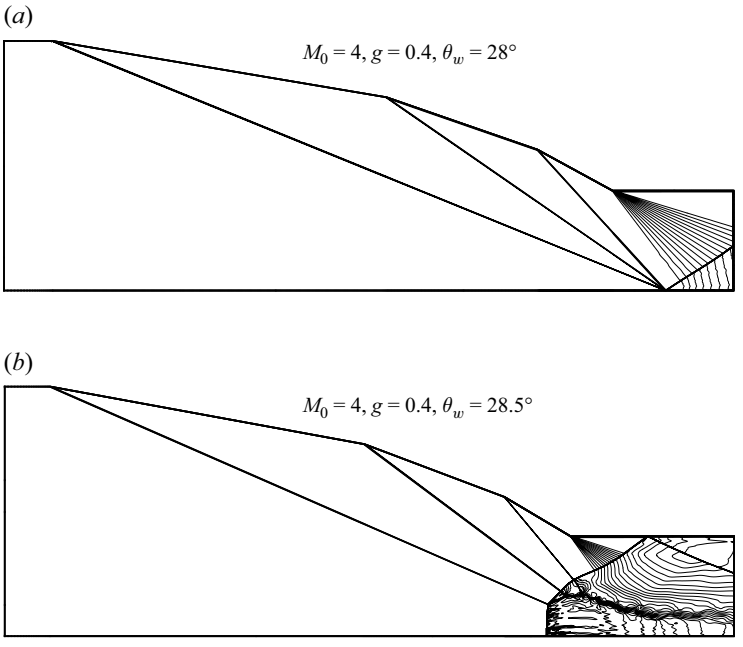


Figure 7. Mach contours with three incident shock waves for $M_0 = 4$: (*a*) $\theta_w = 28°$; (*b*) $\theta_w = 28.5°$.

the von Neumann condition. For this case, we still observe pre-Mach reflection, for the same reason as above.

Next, we will consider the detachment condition. According to figure 5, the detachment conditions are $\theta_{A_1}^{(D)} = 25.61°$ for the first incident shock, $\theta_{A_2}^{(D)} = 27.72°$ for the second incident shock and $\theta_{A_3}^{(D)} = 28.28°$ for the third incident shock.

Figure 7(*a*) displays the numerical results for $\theta_{A_1} = 9.33°$, $\theta_{A_2} = 18.67°$ and $\theta_{A_3} = 28°$, which are all below the detachment conditions for the corresponding incident shocks. As shown in figure 7(*a*), we can observe regular reflection.

Figure 7(*b*) displays the numerical results for $\theta_{A_1} = 9.5°$, $\theta_{A_2} = 19°$ and $\theta_{A_3} = 28.5°$. The wedge deflection angles for the first and second incident shocks are below the detachment conditions, but the wedge deflection angle for the third incident shock is above the detachment condition. In this case, we can no longer observe regular reflection, but rather a pre-Mach reflection.

3.3. *Numerical simulation of shock reflection for various K, observation of shock interaction train*

Figures 8–10 display the Mach contourlines for $M_0 = 4$ and $\theta_w = 30°$, with K varying from 1 to 10. The purpose is to observe how the reflection configuration, particularly the Mach stem height, depends on K. In shock reflection with $K = 1$, if g is smaller than a certain value so that the reflected shock wave touches the shock-generating wedge, then there is no stable shock reflection (Li & Ben-Dor 1997). Note that with various K, we cannot hold the same value for g since the g required to avoid the reflected shock wave interacting with the wedge lower surface is not the same.

The cases with $K = 1$ and $K = 2$ have been studied before and can thus be considered as the familiar ones to start with the discussion on the influence of K. For $K = 1$, we choose $g = 0.55$ and observe Mach reflection according to the Mach contourlines shown

https://doi.org/10.1017/jfm.2025.136 Published online by Cambridge University Press

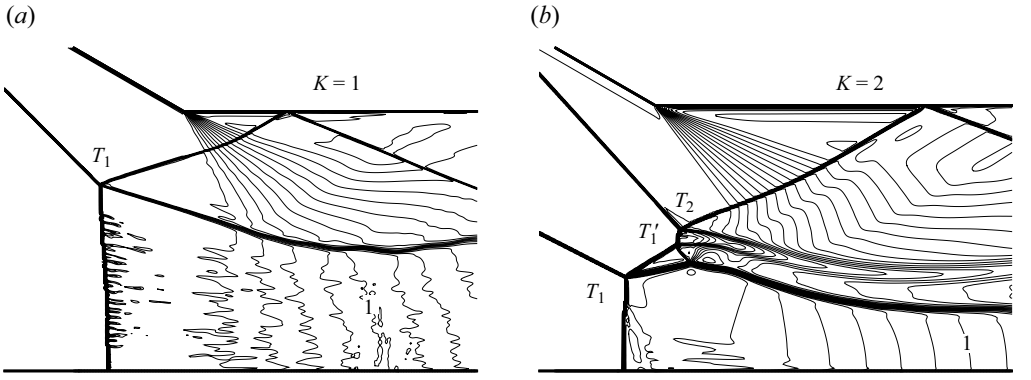


Figure 8. Shock reflection for $M_0 = 4$, $\theta_w = 30°$; (*a*) $g = 0.55$, $K = 1$; (*b*) $g = 0.45$, $K = 2$.

in figure 8(*a*). For $K = 2$, we choose $g = 0.45$ and observe a complex Mach reflection according to the Mach contourlines shown in figure 8(*b*), with three triple points. This situation is regarded as pre-Mach reflection in § 2.1 and in the work of Guan *et al.* (2020), where the first incident shock has Mach reflection while the second incident shock interacts with the reflected shock to generate type-I or type-II shock interference (see Guan *et al.* 2020, for the possibility that both occur under the same condition). According to the discussion in § 2.3, this configuration may also be regarded as post-Mach reflection, with the first incident shock interacting with its Mach stem to produce a type-IV shock interference.

We now look at the results for $K = 3$ to $K = 6$, for which the Mach contourlines with $g = 0.4$ are displayed in figure 9.

For $K = 3$, the result is shown in figure 9(*a*). We have a pre-Mach reflection (a first incident shock Mach reflection, with triple point denoted as T_1), followed by two type-I shock interferences between the reflected shock from triple point T_1 and the second and third incident shocks.

For $K = 4-6$, the Mach contourlines are shown in figures 9(*b*), 9(*c*) and 9(*d*), respectively. We have pre-Mach reflections, followed by a type-II shock interference (instead of type I as observed for $K = 3$), which is generated by the interaction of the second incident shock and the reflected shock from the triple point T_1.This is further followed by several type-I shock interferences, which are generated by the interaction of the third to Kth incident shocks and the reflected shock from the triple point T_1.

We now look at the results for larger K, i.e. $K = 7-10$, for which the Mach contourlines with $g = 0.4$ are displayed in figure 10. We observe pre-Mach reflection as for smaller K, but with the interaction at all the other interaction points being of type-I shock interferences. Thus, the shock reflection begins with a pre-Mach reflection, followed by $(K - 1)$ type-I shock interferences when K reaches a certain value. The reason that we no longer have type-II shock interference is that the increase of K weakens the strength of the incident shocks, making it difficult for the second to Kth incident shocks to generate type-II shock interference.

Consider $K = 6$, for which we observe type-II interference at point T_2. The reflected shock from T_1 has a shock angle $\beta = 19.52°$ and the second incident shock has a shock angle $\beta = 19.52°$, with an upstream Mach number of 3.63. Now, for $K = 7$, we observe type-I reflection at point T_2. The reflected shock from T_1 has a shock angle $\beta = 18.74°$ and the second incident shock has a shock angle $\beta = 18.74°$, with an upstream Mach number of 3.69. The reflection between two shocks of the same family defines asymmetric shock

https://doi.org/10.1017/jfm.2025.136 Published online by Cambridge University Press

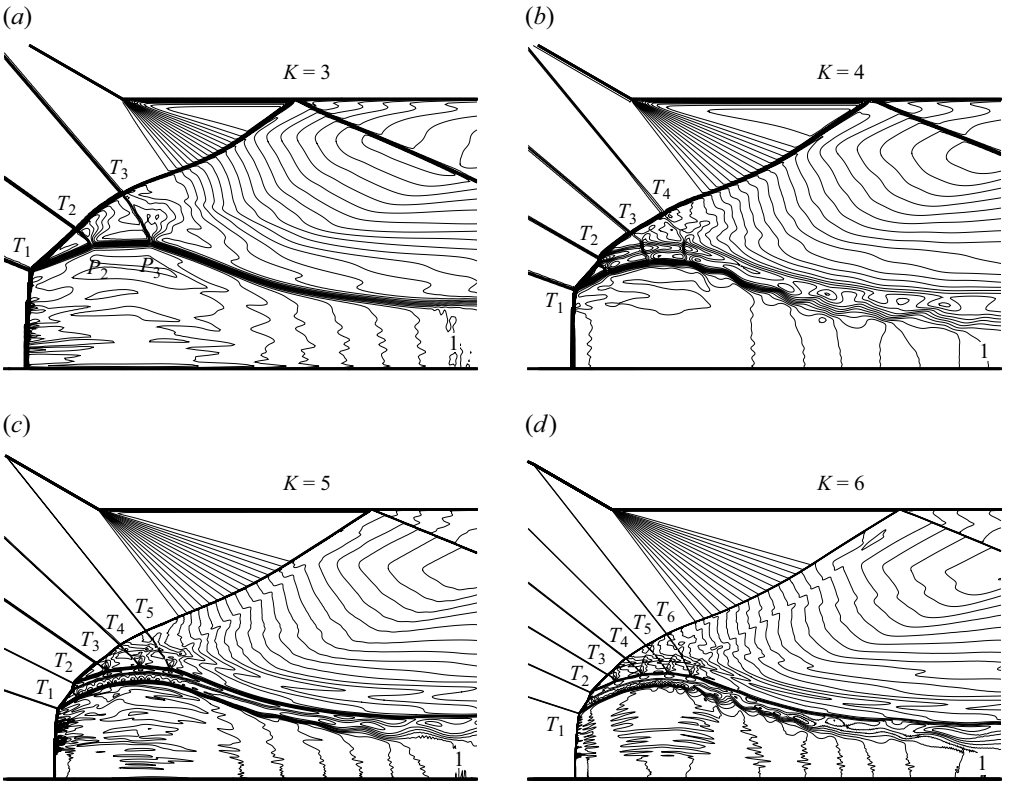


Figure 9. Shock reflection for $M_0 = 4$, $\theta_w = 30°$, $g = 0.4$: (*a*) $K = 3$; (*b*) $K = 4$; (*c*) $K = 5$; (*d*) $K = 6$.

reflection, as studied by Li, Chpoun & Ben-Dor (1999). For each inflow Mach number, whether we have type-I or type-II shock interferences depends on the shock angles of the two incident shock waves. However, Li *et al.* (1999) only provide transition conditions when the inflow Mach number is 4.96.

The term 'shock interaction train' may be used to define the configuration of shock reflection as shown in figures 8–10. The shock interaction train has a pre-Mach reflection for the first incident shock, followed by a series of type-I or type-II shock interferences for the second to Kth incident shocks. Figure 11 provides a schematic display of the shock interaction train, including pure type-I shock interference (figure 11*a*), pure type-II shock interference (figure 11*b*) and hybrid type I–II shock interference (figure 11*c*).

Now, we consider how the Mach stem height depends on K. Even for single incident shock reflection, the mechanism to determine the size of the Mach reflection configuration has been considered as a challenging problem, as described by Ben-Dor (2007) p. 53 and addressed by Hornung & Robinson (1982). They argued that the Mach stem height is affected by the pressure decrease information from the wedge trailing edge expansion fan. Hornung & Robinson (1982) postulated a functional form of the Mach stem height, showing that the relative height of the Mach stem (H_T/w) depends on M_0, θ_w, γ and H_R/w (the relative trailing edge height), i.e.

$$\frac{H_T}{w} = f\left(M_0, \theta_w, \gamma, \frac{H_R}{w}\right), \tag{3.16}$$

where H_T is the vertical distance from the triple point to the reflecting surface. Actually, according to the geometrical relation $w = (H_{A_0} - H_R)\tan\theta_w$, (3.16) can be rewritten as

https://doi.org/10.1017/jfm.2025.136 Published online by Cambridge University Press

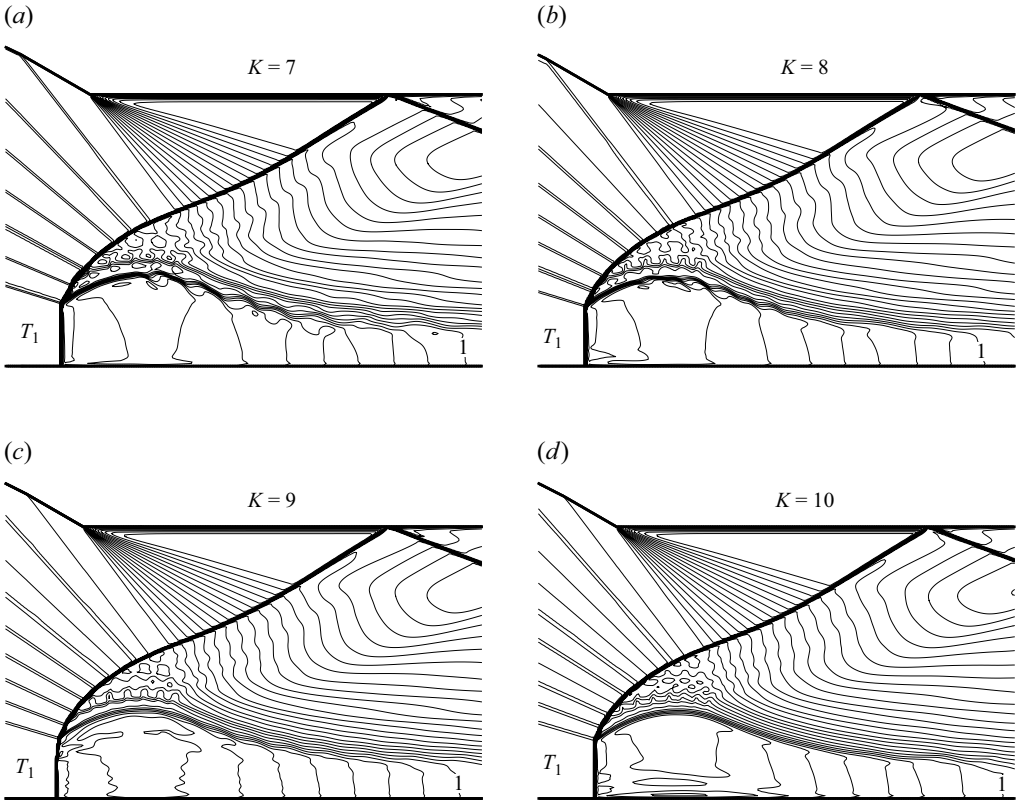


Figure 10. Shock reflection for $M_0 = 4$, $\theta_w = 30°$, $g = 0.4$: (*a*) $K = 7$; (*b*) $K = 8$; (*c*) $K = 9$; (*d*) $K = 10$.

$$\frac{H_T}{H_{A_0}} = f(M_0, \theta_w, \gamma, g), \tag{3.17}$$

where g $(= H_R/H_{A_0})$ is the relative trailing edge height. For the present problem, the relative height of Mach stem (H_{T_1}/H_{A_0}) should also depend on K, so we would have

$$\frac{H_{T_1}}{H_{A_0}} = f(M_0, \theta_w, \gamma, g, K), \tag{3.18}$$

where H_{T_1} is the vertical distance from the triple point T_1 to the reflecting surface. The explicit form of (3.18) is rather complex to obtain, since even in the single incident shock reflection problem, the model to estimate H_T has been a challenging issue that has attracted numerous studies, starting from the work of Azevedo (1989) and Azevedo & Liu (1993). The model relies on the use of triple-shock theory, the method to describe the characteristics that bring the trailing edge pressure into the sonic throat below the slipline and a quasi-one-dimensional modelling for the flow below the slipline. Since the pioneering studies by Azevedo & Liu (1993), further elaboration has been considered to improve the modelling (cf. Li & Ben-Dor 1997; Mouton & Hornung 2007; Gao & Wu 2010; Bai & Wu 2017; Chernyshov, Savelova & Kapralova 2021; Choe 2022) and to extend it to more complex flows (cf. Schotz *et al.* 1997; Grasso & Paoli 1999; Shoesmith & Timofeev 2021; Vinoth, Sushmitha & Rajesh 2022).

https://doi.org/10.1017/jfm.2025.136 Published online by Cambridge University Press

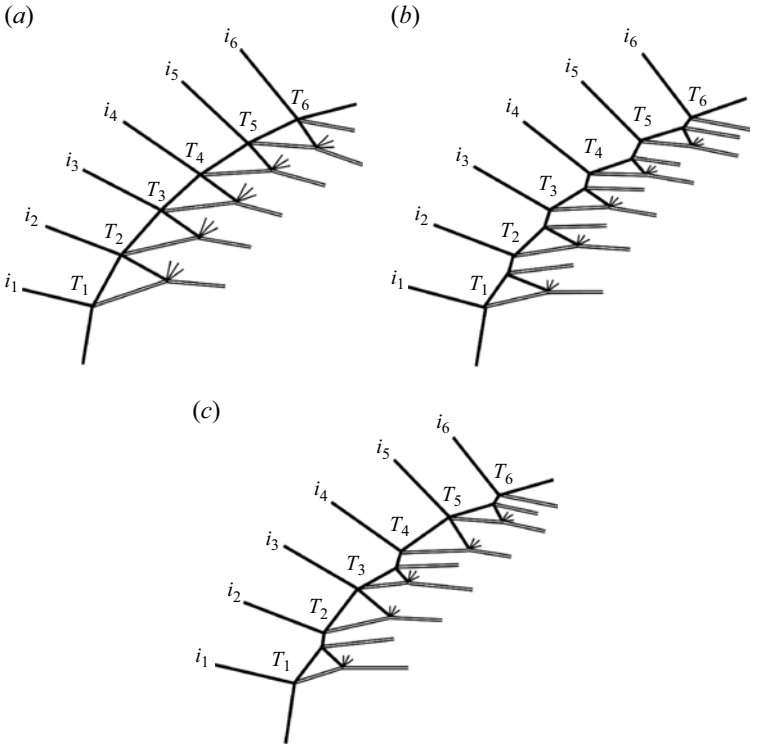


Figure 11. Possible shock interaction train: (*a*) pure type-I shock interference; (*b*) pure type-II shock interference; (*c*) mixed type-I–II shock interferences.

K	H_{T_1}/H_{A_0}	$H_{highest}/H_{A_0}$	H_{throat}/H_{A_0}
1	0.3928	0.3928	0.2591
2	0.1589	0.1805	0.1041
3	0.1415	0.1789	0.0912
4	0.1176	0.1568	0.0759
5	0.1041	0.1442	0.0663
6	0.0973	0.1382	0.0629
7	0.0932	0.1347	0.0611
8	0.0884	0.1298	0.0586
9	0.0881	0.1297	0.0578
10	0.0877	0.1282	0.0568

Table 4. Variation of several normalised heights with K for $M_0 = 4$, $\theta_w = 30°$.

Let us take a look at the specific variation of Mach height with K. Table 4 presents the normalised Mach stem height of the first interaction point T_1 (H_{T_1}/H_{A_0}), the normalised height of the highest point of the quasi one-dimensional duct ($H_{highest}/H_{A_0}$) from T_1, and the normalised height of the throat of the duct (H_{throat}/H_{A_0}) from T_1 for $M_0 = 4$ and $\theta_w = 30°$, with K varying from 1 to 10. We choose $g = 0.55$ for $K = 1$, $g = 0.45$ for $K = 2$ and $g = 0.4$ for $K = 3-10$. So the results for $K = 1$ and $K = 2$ cannot be compared with the results for other K due to variations in g. From table 4, we can observe the following information:

https://doi.org/10.1017/jfm.2025.136 Published online by Cambridge University Press

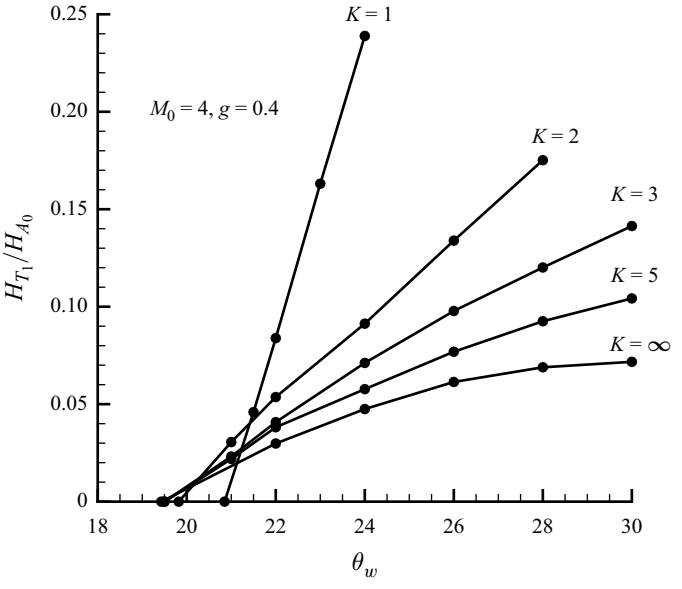


Figure 12. Normalised Mach stem height of the first interaction point H_{T_1}/H_{A_0} with $M_0 = 4$, $g = 0.4$ and different K.

(1) the normalised Mach stem height decreases as K increases, and the rate of decrease slows down;
(2) the normalised height of the highest point of the quasi one-dimensional duct decreases as K increases, and the rate of decrease slows down;
(3) the normalised height of the throat of the duct decreases as K increases, and the rate of decrease slows down.

The above variation can be heuristically understood. For the single shock wave reflection problem, when the incoming Mach number M_0 is fixed, the normalised Mach stem height decreases as wedge deflection angle θ_w increases (Gao & Wu, 2024). For the multiple incident shock reflection problem, when the incoming Mach number M_0 is fixed, increasing K and increasing θ_w have similar effects based on the parameters downstream of the Kth incident shock. For example, both will lead to a decrease in Mach number and an increase in pressure jump downstream of the Kth incident shock wave. Therefore, it is inferred that increasing K in multiple incident shock reflection will have a similar effect as increasing θ_w in single shock wave reflection, that is, causing an increase in the normalised Mach stem height and other similar normalised heights.

Figure 12 shows the variations in normalised Mach stem height H_{T_1}/H_{A_0} as a function of the total wedge deflection angle θ_w for $M_0 = 4$, $g = 0.4$ and $K = 1, 2, 3, 5, \infty$. The normalised Mach stem height decreases as K increases in most ranges of θ_w. However, there are some intersection points between different lines when the total wedge deflection angle θ_w is near the von Neumann condition, indicating that the laws of variation will become complex. In addition, for $K = 2$, the normalised Mach stem height varies almost linearly with θ_w, similar to $K = 1$. As K increases, the variation patterns become nonlinear and get closer to the result of $K = \infty$.

Through the transition criteria displayed in figure 5, we can see that for the same inflow Mach number M_0, a larger K results in a smaller von Neumann condition. Therefore, when θ_w is small and close to the von Neumann condition, if K is less than a specific value, the

https://doi.org/10.1017/jfm.2025.136 Published online by Cambridge University Press

reflection is in the regular reflection domain, which means the Mach stem height will be zero. If K is greater than that specific value, the reflection is in the double solution domain, which means the Mach stem height will be larger than zero. Therefore, when θ_w is small enough, the normalised Mach stem height will no longer decrease as K increases. This reversal phenomenon of Mach stem height variation has occurred in the reflection of a centred compression wave for the same reason, as shown in figure 13 of Bai (2024). We can see that the Mach stem height for centred compression wave reflection is lower than shock wave reflection in most situations, but it becomes higher when θ_w is small enough (approximately 21° for $M_0 = 4$).

4. Concluding remarks

In this paper, we have studied the reflection of K incident shock waves in steady supersonic flow, focusing on the case where all the incident shocks reflect at the same point. The total number of possible reflection types is evaluated by counting, at each shock interaction point, the number of possible shock reflections or interference patterns. The von Neumann condition and the detachment condition for multiple shock reflection with equal variation of deflection angles are obtained for each incident shock. Numerical simulations are used to study the shock reflection configuration for K up to 10.

The reflection type of multiple incident shocks can be roughly divided into regular reflection and Mach reflection. Mach reflection is very complex because it includes various shock reflection and shock interference structures. If the kth incident shock has Mach reflection and the first $(k-1)$ incident shocks generate type-IV shock interaction and the last $(K-k)$ incident shocks generate type-I or type-II shock interference, then the estimated number of possible Mach reflection configurations is $2^K - 1$. However, if we consider the similarity between different configurations, then all the Mach reflections can be regarded as a pre-Mach reflection followed by $(K-1)$ type-I or type-II shock interferences, so the total number of possible Mach reflection configurations is reduced to 2^{K-1}.

For multiple shock reflection with equal variation of deflection angles, we have obtained the transition conditions in the $\theta_w - M_0$ plane, from which we see that the von Neumann condition for the kth incident shock is lower than that of classical shock reflection and decreases further as k increases, while the detachment condition for the kth incident shock is higher than that of classical shock reflection and increases further as k increases, i.e. the region of the double solution domain increases as k increases and tends to the region for a centred compression wave reflection when k approaches infinity.

Numerical simulations are used to study the Mach reflection structure for $K = 1, 2, \ldots, 10$. According to the numerical results, the Mach reflection configuration is a shock interaction train that begins with a pre-Mach reflection and is followed by $(K-1)$ type-I–II interference structures. For the condition considered, the normalised Mach stem height decreases as K increases while the other parameters are fixed.

The present study bridges the two extreme cases with $K = 1$ and $K = \infty$. The case with $K = 1$ is the classical shock reflection one that has been well studied before (Ben-Dor 2007). The case with $K = \infty$ has been studied recently for the special case of a centred compression wave (Bai 2024), which may be regarded as composed of an infinite number of incident shocks of equal deflection angle.

Funding. This work was supported by the National Natural Science Foundation of China (nos 12472232 and 52192632), the Young Elite Scientist Sponsorship Program by CAST (no. YESS20210042) and the Young Talent Support Plan of Beihang University.

https://doi.org/10.1017/jfm.2025.136 Published online by Cambridge University Press

Declaration of interests. The authors report no conflict of interest.

References

AZEVEDO, D.J. 1989 Analytical prediction of shock patterns in a high-speed wedge bounded duct. PhD thesis, Dept. Mech. & Aero. Engng, State University NY, Buffalo.

AZEVEDO, D.J. & LIU, C.S. 1993 Engineering approach to the prediction of shock patterns in bounded high-speed flows. *AIAA J.* **31** (1), 83–90.

BAI, C.Y. & WU, Z.N. 2017 Size and shape of shock waves and slipline for Mach reflection in steady flow. *J. Fluid Mech.* **818**, 116–140.

BAI, C.Y. 2024 Reflection of a centred compression wave. *J. Fluid Mech.* **984**, A3.

BEN-DOR, G., IVANOV, M., VASILEV, E.I. & ELPERIN, T. 2002 Hysteresis processes in the regular reflection to Mach reflection transition in steady flows. *Prog. Aerosp. Sci.* **38** (4-5), 347–387.

BEN-DOR, G. 2007 *Shock Wave Reflection Phenomena*. Springer.

BUSEMANN, A. 1942 Die achsensymmetrische kegelige Uberschallstromung. *Luftfahrtforschung* **19**, 137–144.

CHERNYSHOV, M.V., SAVELOVA, K.E. & KAPRALOVA, A.S. 2021 Approximate analytical models of Shock-Wave structure at steady Mach reflection. *Fluids* **6** (9), 305.

CHOE, S.G. 2022 A method for predicting Mach stem height in steady flows. Proceedings of the Institution of Mechanical Engineers, Part G. *J. Aerosp. Engng* **236** (1), 3–10.

CHPOUN, A., PASSEREL, D., LI, H. & BEN-DOR, G. 1995 Reconsideration of oblique shock wave reflections in steady flows. Part 1. Experimental investigation. *J. Fluid Mech.* **301**, 19–35.

GAO, B. & WU, Z.N. 2010 A study of the flow structure for Mach reflection in steady supersonic flow. *J. Fluid Mech.* **656**, 29–50.

GRASSO, F. & PAOLI, R. 1999 An analytical study of Mach reflection in nonequilibrium steady flows. *Phys. Fluids* **11** (10), 3150–3167.

GUAN, X.K., BAI, C.Y. & WU, Z.N. 2018 Steady Mach reflection with two incident shock waves. *J. Fluid Mech.* **855**, 882–909.

GUAN, X.-K., BAI, C.-Y. & WU, Z.-N. 2020 Double solution and influence of secondary waves on transition criteria for shock interference in pre-Mach reflection with two incident shock waves. *J. Fluid Mech.* **887**, A22.

GUAN, X.K., BAI, C.Y., LIN, J. & WU, Z.N. 2020 Mach reflection promoted by an upstream shock wave. *J. Fluid Mech.* **903**, A44.

HEKIRI, H. & EMANUEL, G. 2015 Structure and morphology of a triple point. *Phys. Fluids* **27** (5), 056102.

HORNUNG, H.G., OERTEL, H. & SANDEMAN, R.J. 1979 Transition to Mach reflection of shock waves in steady and pseudo-steady flows with and without relaxation. *J. Fluid Mech.* **90** (3), 541–560.

HORNUNG, H.G. & ROBINSON, M.L. 1982 Transition from regular to Mach reflection of shock waves Part 2. The steady-flow criterion. *J. Fluid Mech.* **123**, 155–164.

IVANOV, M.S., VANDROMME, D., FOMIN, V.M., KUDRYAVTSEV, A.N., HADJADJ, A. & KHOTYANOVSKY, D.V. 2001 Transition between regular and Mach reflection of shock waves: new numerical and experimental results. *Shock Waves* **11** (3), 199–207.

LI, H. & BEN-DOR, G. 1997 A parametric study of Mach reflection in steady flows. *J. Fluid Mech.* **341**, 101–125.

LI, H., CHPOUN, A. & BEN-DOR, G. 1999 Analytical and experimental investigations of the reflection of asymmetric shock waves in steady flows. *J. Fluid Mech.* **390**, 25–43.

MACH, E. 1878 Uber den verlauf von Funkenwellen in der Ebene und im Raume. *Sitzungsbr Akad Wiss Wien.* **78**, 819–838.

MOUTON, C.A. & HORNUNG, H.G. 2007 Mach stem height and growth rate predictions. *AIAA J.* **45**, 1977–1987.

OGAWA, H., MODER, S., TIMOFEEV, E.V. & BOYCE, R.R. 2015 Startability and Mach Reflection Hysteresis of Shortened Busemann Intakes for Axisymmetric Scramjet Engines. In *29th International Symposium on Shock Waves 1*, pp. 641–646. Springer.

ROYE, L., HENDERSON, F. & MENIKOFF, R. 1998 Triple-shock entropy theorem and its consequences. *J. Fluid Mech.* **366**, 179–210.

SCHOTZ, M., LEVY, A., BEN-DOR, G. & IGRA, O. 1997 Analytical prediction of the wave configuration size in steady flow Mach reflections. *Shock Waves* **7** (6), 363–372.

SHOESMITH, B. & TIMOFEEV, E. 2021 Modelling of Mach reflections in internal axisymmetric steady supersonic flow. *Shock Waves* **31** (8), 945–957.

VINOTH, P., SUSHMITHA, J. & RAJESH, G. 2022 Prediction of Mach stem height in compressible open jets. Part 1. Overexpanded jets. *J. Fluid Mech.* **942**, A48.

https://doi.org/10.1017/jfm.2025.136 Published online by Cambridge University Press

VON NEUMANN, J. 1943 Oblique reflection of shock. *Explos. Res. Rep.* 12. Navy Department, Bureau of Ordinance.

VON NEUMANN, J. 1945 Refraction, intersection and reflection of shock waves. *NAVORD Rep.* 203-245. Navy Department, Bureau of Ordinance.

VUILLON, J., ZEITON, D. & BEN-DOR, G. 1995 Reconstruction of oblique shock wave reflection in steady flows. Part 2. Numerical investigation. *J. Fluid Mech.* **301**, 37–50.

https://doi.org/10.1017/jfm.2025.136 Published online by Cambridge University Press